Dynamic Cell Association for Non-Orthogonal Multiple-Access V2S Networks

Li Ping Qian, *Senior Member, IEEE*, Yuan Wu, *Senior Member, IEEE*,
Haibo Zhou, *Member, IEEE*, and Xuemin Shen, *Fellow, IEEE*

***Abstract*— To meet the growing demand of mobile data traffic in vehicular communications, the vehicle-to-small-cell (V2S) network has been emerging as a promising vehicle-to-infrastructure technology. Since the non-orthogonal multiple access (NOMA) with successive interference cancellation (SIC) can achieve superior spectral and energy efficiency, massive connectivity and low transmission latency, we introduce the NOMA with SIC to V2S networks in this paper. Due to the fast vehicle mobility and varying communication environment, it is important to dynamically allocate small-cell base stations and transmit power to vehicular users with considering the vehicle mobility in NOMA-enabled V2S networks. To this end, we present the joint optimization of cell association and power control that maximizes the long-term system-wide utility to enhance the long-term system-wide performance and reduce the handover rate. To solve this optimization problem, we first equivalently transform it into a weighted sum rate maximization problem in each time frame based on the standard gradient-scheduling framework. Then, we propose the hierarchical power control algorithm to maximize the equivalent weighted sum rate in each time frame based on the Karush–Kuhn–Tucker (KKT) optimality conditions and the idea of successive convex approximation. Finally, theoretical analysis and simulation results are provided to demonstrate that the proposed algorithm is guaranteed to converge to the optimal solution satisfying KKT optimality conditions.**

***Index Terms*— Non-orthogonal multiple access, successive interference cancellation, vehicle-to-small-cell network, joint optimization of cell association and power control, long-term system-wide utility maximization.**

I. Introduction

TO COPE with the unprecedented growth of wireless data traffic in recent years, the small cell networking topology has been emerging as a promising and scalable solution to improve spectrum and energy efficiency as well as expand indoor and cell-edge coverage in future fifth-generation (5G) cellular networks [1]–[6]. Such a networking topology is to deploy various classes of small-cell/lower-power base stations (BSs) such as picocells, femtocells, and perhaps relays underlaid in a macro-cellular network. Different from traditional wireless networks, vehicular wireless networks are expected to deliver the real-time contents such as monitoring and multimedia streams, and the non-real-time contents such as web-browsing, image, messaging, and file transfers for vehicular users (VUs) [7]. Due to the fast vehicle mobility and varying communication environment, the advanced underlying radio access technologies are indispensable for the reliable data delivery and ubiquitous converge in vehicular wireless networks. Driven by the massive deployment of small cells, the vehicle-to-small-cell (V2S) network is recommended as a promising vehicle-to-infrastructure (V2I) access technology [8], [9]. However, the V2S network suffers from the severe co-channel interference and the unbalanced traffic load distribution among neighbor cells when small cells are ultra densely deployed. Meanwhile, more frequent handover requests would be triggered easily due to the fast vehicle mobility. Therefore, the implementation of V2S networks poses serious challenges, such as the frequent handoff, severe radio frequency interference, and load imbalance, which may lead to inefficient spectrum and energy utilization.

Since the non-orthogonal multiple access (NOMA) technique can support multiple users on the same frequency-time resource simultaneously by non-orthogonal resource allocation in the power domain, it has been actively investigated as a potential alternative to existing orthogonal multiple access (OMA) techniques for 5G cellular networks [10], [11]. In comparison with OMA, the main advantages of NOMA include improved spectral and energy efficiency, massive connectivity, and low transmission latency. Therefore, NOMA can be developed as a proposing multiple access solution to improve the spectral and energy efficiency in V2S networks. Despite the superior benefits of NOMA, it still cannot reduce the handover rate or balance traffic load among cells in V2S networks. A survey on cell association [12] reveals that the cell association optimization technique, namely properly associating a user with a particular serving small-cell BS, plays a pivotal role in enhancing the load balancing and the spectrum and energy efficiency of networks. The handover performance experienced in LTE-A systems further reveals that the cell association optimization technique can effectively reduce the handover rate [14]. Since the communication conditions and the density of VUs per small cell are time-varying in V2S networks due to the fast vehicle mobility, the existing

Manuscript received January 22, 2017; revised April 21, 2017; accepted May 22, 2017. Date of publication July 11, 2017; date of current version September 15, 2017. This work was supported in part by the National Natural Science Foundation of China under Project 61379122, Project 61572440, and Project 91638204, in part by the Zhejiang Provincial Natural Science Foundation of China under Project LR16F010003, Project LR17F010002, and Project LQ15F010003, and in part by the Natural Sciences and Engineering Research Council, Canada. *(Corresponding author: Yuan Wu.)*

L. P. Qian and Y. Wu are with the College of Information Engineering, Zhejiang University of Technology, Hangzhou 310023, China (e-mail: lpqian@zjut.edu.cn; iewuy@zjut.edu.cn).

H. Zhou and X. Shen are with the Department of Electrical and Computer Engineering, University of Waterloo, Waterloo, ON N2L 3G1, Canada (e-mail: h53zhou@uwaterloo.ca; xshen@bbcr.uwaterloo.ca).

Color versions of one or more of the figures in this paper are available online at http://ieeexplore.ieee.org.

Digital Object Identifier 10.1109/JSAC.2017.2725178

cell association schemes such as channel-aware, traffic-load-aware, and transmit-power-aware schemes, may be highly suboptimal and require excessive handovers when applied to V2S networks. Therefore, it is of practical importance to develop a dynamic cell association mechanism that can enhance the load balancing and reduce the handover rate by adaptively taking into account the influence of vehicle mobility in V2S networks.

Although there have been significant efforts dedicated on NOMA, the study on NOMA for V2S networks is surprisingly rare in the open literature. Correspondingly, there is lack of adaptive optimal cell association in NOMA-enabled V2S networks. Motivated by these gaps, in this paper, we consider a downlink V2S network consisting of multiple small-cell BSs deployed along the road sides and VUs moving on the road, in which all small-cell BSs and VUs are equipped with a single antenna each and all channel state information (CSI) related to VUs is perfect to each small-cell BS. Typically, the CSI can be collected by estimating it at the side of VU and sending it to the corresponding small-cell base station via a feedback channel [13]. Driven by the superior spectrum and energy efficiency, we introduce the NOMA with SIC to the downlink V2S network, in which every BS simultaneously serves multiple VUs via superposition coding, and every VU adopts the SIC receiver to decode its signal from its associated BS. Using NOMA with SIC, every VU can eliminate some of the co-channel interference by the SIC receiver so that the spectrum and energy efficiency of V2S network can be effectively improved. Considering the vehicle mobility, it is significant to dynamically allocate small-cell base stations (BSs) and transmit power to VUs which perceive different channel gains to small-cell BSs. Such an operation can enhance the long-term system-wide performance and avoid excessive handovers. This leads us to the concept of joint optimization of cell association and power control, which is essentially the power-updating based re-association/handover problem for NOMA-enabled V2S networks. In particular, the main contributions of this paper are summarized as follows:

- *NOMA With SIC:* We apply the NOMA scheme with SIC for downlink V2S networks. While the out-of-cell interference has to be considered, an SIC receiver at each VU is used to decode its own information through mitigating some of in-cell interference.
- *Novel Problem Formulation:* We present the joint optimization of cell association and power control problem on maximizing the system-wide utility with respect to the long-term average data rate obtained by each small-cell BS subject to the upper bound of small-cell BSs' power consumption. In this doing, the cell association and power control can be adaptive to the traffic load conditions in the small cells and the fast vehicle mobility.
- *Efficient Algorithm Design:* The optimal solution of maximizing the network-wide utility can be equivalently transformed into a weighted sum rate maximization problem in each time frame based on a standard gradient-based algorithm, through exploring the convex nature of the joint optimization. The equivalent weighted sum rate maximization problem is in general non-convex due to the mutual coupling among the out-of-cell interference of all VUs. We therefore propose a hierarchical power control algorithm to maximize the weighted sum rate across small-cell BSs in each time frame based on the Karush-Kuhn-Tucker (KKT) optimality conditions and the idea of successive convex approximation. Our proposed algorithm is guaranteed to converge to the optimal solution satisfying KKT optimality conditions. Considering the vehicle mobility, the decisions on optimal power allocation for small-cell BSs and VUs are made according to the real-time network environment in each time frame.

The remainder of the paper is organized as follows. Section II summarizes the related work on NOMA with SIC and cell association in wireless communication networks. Section III introduces the system model about the downlink NOMA-enabled V2S network, and problem formulation on the joint optimization of cell association and power control. Section IV proposes the hierarchical power control algorithm to dynamically optimize the transmit power levels of small-cell BSs and VUs based on a standard gradient-based framework. Section V evaluates the performance of the proposed algorithm through several simulations. Section VI concludes this paper.

II. Related Work

In this paper, we introduce two techniques, e.g., the NOMA with SIC and the cell association, to V2S networks for improving the spectrum and energy efficiency, balancing the traffic load distribution, and reducing the handover rate. Therefore, we review the existing work on these two techniques in this section.

A. NOMA With SIC

Due to the advantages including improved spectral and energy efficiency, massive connectivity, and low transmission latency, NOMA with SIC has attracted lots of research interests for 5G wireless networks in the literature [15]–[21], which can be divided into two threads. The first concern is about performance investigation for wireless networks using NOMA with SIC. For example, the capacity region of the two-user network was derived in the context of NOMA with SIC [15]. Reference [16] derived the user transmission rate when NOMA with SIC was employed in a downlink coordinated cellular network. Reference [17] carried out the evaluation of the outage probability and ergodic sum rates for a downlink NOMA-SIC cellular network when considering fixed power allocation. The impact of user paring on the performance was evaluated for NOMA with fixed power allocation and cognitive-radio-inspired NOMA in [18]. Apart from the performance investigation, more research attentions have been paid to resource allocation in wireless networks using NOMA with SIC. For example, [19] maximized the sum-rate utility via the joint optimization of power and channel allocation for the downlink NOMA-SIC cellular network. Reference [20] maximized the minimum achievable user rate through appropriate power allocation among users for the downlink NOMA-SIC cellular network. In the uplink NOMA-SIC cellular network,

the optimal power allocation was studied for the maximum throughput scheduling and proportional fairness scheduling in [21]. Although significant effort has been put on NOMA with SIC, there is not much study on network performance when NOMA with SIC is applied to V2S networks. In this work, we study how to improve the network performance when applying NOMA with SIC to the V2S network.

B. Cell Association

On the one hand, the unbalanced traffic load distribution and sever co-channel interference among cells lead to inefficient spectrum and energy utilization. On the other hand, the V2S network is expected to perform massive connectivity, low handover latency, and infrequent handovers. To meet these challenges, the cell association (conventionally, handover/handoff) that can adapt to the traffic load conditions in the small cells and the fast vehicle mobility has attracted extensive research efforts [14], [22]–[28]. Without loss of generality, these studies can be broadly classified into two categories. The first category concerns the performance evaluation on cell association mechanisms [14], [22]. The handoff rate and coverage analysis was performed in [14] for a multi-tier small cell network with orthogonal spectrum allocation among tiers and the maximum biased average received power as the tier association metric. A new stochastic geometric analysis framework on user mobility was proposed in [22] to quantify the rates of horizontal and vertical handoffs, under random multi-tier BSs, arbitrary user movement trajectory, and flexible user-BS association. The second category concerns the design of cell association mechanisms [23]–[28]. Initially, the cell association was studied without accounting for resource management [23]–[26]. Work [23] proposed the cell association mechanism for minimizing packet losses during handoffs, and [24] proposed the cell association mechanism for reducing handoff delay. Arshad *et al.* [25], proposed a velocity-aware handover management scheme for two-tier downlink cellular networks to mitigate the handover effect on the foreseen densification throughput gains. In [26], a user centered handoff scheme was proposed to maximize the achievable receiving data rate and minimize the block probability simultaneously for 5G networks. After that, the cell association mechanism was designed jointly with resource allocation for wireless networks [27], [28]. Fang and Zhou [27], proposed a joint bandwidth allocation and call admission control (CAC) strategy to reduce high-mobility users' handovers based on the stochastic geometry modeling. Reference [28] proposed a cell association mechanism jointly with channel timeline allocations to provide fair long-term throughput for the users.

Despite significant efforts spent on cell association, there is few work realizing the cell association that adapts to the influence of vehicle mobility from the perspective of long-term system-wide utility. Furthermore, these work applied either the orthogonal multiple access (e.g., orthogonal frequency division multiple access) or the traditional non-orthogonal multiple access (i.e., pure power control). Motivated by these, it is important to address the joint optimization of cell association and resource allocation that maximizes the long-term system-wide utility, when the NOMA with SIC is applied to V2S networks.

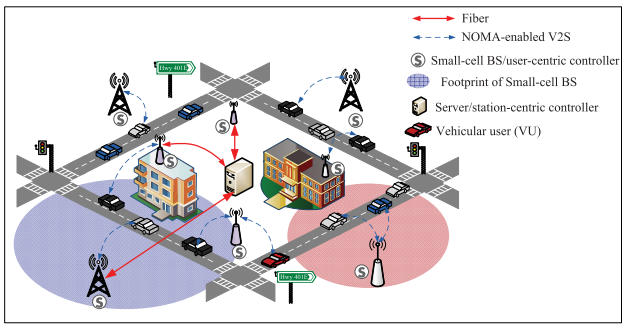

Fig. 1. Downlink NOMA-enabled V2S network consisting of a set of small-cell BSs deployed along the road sides and a set of vehicular users moving on the road, in which all small-cell BSs are connected to the server established by the mobile network operator via fiber.

III. System Model and Problem Formulation

A. System Model

We consider a downlink NOMA-enabled V2S network as shown in Fig. 1. The V2S network consists of a set of $\mathcal{S} = \{1, 2, \cdots, S\}$ of small-cell BSs deployed along the road sides and a set $\mathcal{M} = \{1, 2, \cdots, M\}$ of vehicular users (VUs) moving on the road. Let $\boldsymbol{y}_s$ denote the location of small-cell BS s. We use the trace of VU m on the move to model its mobility process, i.e., $\{\boldsymbol{x}_{m,t}\}_{t=1,\cdots}$, where $\boldsymbol{x}_{m,t}$ indicates the location of VU m at the beginning of time frame t. Both small-cell BSs and VUs are assumed to be equipped with a single antenna each. The total channel bandwidth is B Hz, and is shared among the M VUs in the NOMA manner. In particular, we apply the NOMA with SIC to V2S networks, in which each VU is equipped with an SIC receiver. The SIC receiver of VU m performs SIC to decode the received signal of VU m after sequentially decoding the received signals intended for VUs associated to small-cell BS s but with lower interference-cancellation order than VU m. However, the received signals intended for VUs associated to small-cell BS s but with higher interference-cancellation order than VU m and the received signals from all other active small-cell BSs are treated as interference at the receiver of VU m when performing SIC. Considering the inter-cell interference, the interference-cancellation ordering of VUs associated to one small-cell BS is determined in the increasing order of channel-gain-to-inter-cell-interference-plus-noise ratio of these VUs, where the channel gain of one VU means the one between the associated small-cell BS and this VU. The transmission is on a time-frame basis, with each frame consisting of multiple data symbols. Every small-cell BS synchronizes the transmissions of its associated VUs in each time frame. We assume that the channel gain coefficients of all VUs are frequency-flat across the whole bandwidth, and unchanged within each time frame but can vary from one frame to another due to VUs' mobility and fading effects.

Considering the vehicle mobility, it is significant to dynamically allocate small-cell BSs to VUs through adjusting the

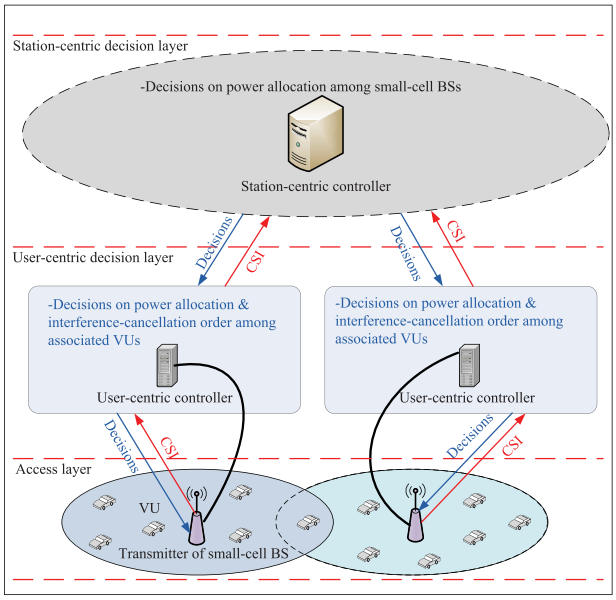

Fig. 2. Framework of downlink NOMA-enabled V2S network.

transmit power of each small-cell BS and the power allocation among its associated VUs. To this end, we present the framework of downlink NOMA-enabled V2S communications for the power control in Fig. 2. Such a V2S communication network covers two decision layers: the station-centric decision layer and the user-centric decision layer. The station-centric layer includes the station-centric controller, to which all small-cell BSs are connected via fiber. The station-centric controller is in charge of determining the total amount of power to be transmitted by each small-cell BS based on CSI. The user-centric decision layer is close to VUs, and includes user-centric controllers embedded with small-cell BSs. The user-centric controller allocates the determined total amount of power among the data streams to its associated VUs and determines the interference cancellation order of each associated VU according to CSI. The resulting power allocation is used to configure the encoder at the transmitter of small-cell BS, and the resulting interference cancellation order facilitates the decoder at each associated VU.

B. Problem Formulation

Let $P_{s,t}$ denote the total transmit power of small-cell BS s which is used to transmit data symbols to its all associated VUs in time frame t, with $P_{s,\max}$ being its maximum allowable value. Note that small-cell BS s is off in time frame t if its transmit power $P_{s,t}$ is equal to zero, and is on otherwise. Let $p_{sm,t}$ denote the transmit power with which small-cell BS s transmits the data symbols of VU m in time frame t. Note that VU m is associated with small-cell BS s in time frame t only when the transmit power $p_{sm,t}$ is positive. Therefore, *we can integrate the on/off small-cells strategy and the cell association strategy together through controlling the transmit power of small-cell BSs and VUs*. We use $g_{sm,t}$ to denote the channel gain between small-cell BS s and VU m in time frame t, which is generally determined by path loss and fading effects. Specifically, $g_{sm,t}$ is formulated as the function $G(\cdot)$:

$$g_{sm,t} = G(||\boldsymbol{x}_{m,t} - \boldsymbol{y}_s||, f_{sm,t}), \tag{1}$$

where $||\boldsymbol{x}_{m,t} - \boldsymbol{y}_s||$ and $f_{sm,t}$ mean the distance and fading effect between VU m and small-cell BS s in time frame t, respectively. In the practical V2S network, the fading effect of VU m is mainly subject to the large obstructions around its moving trace and its velocity. Assuming that VU m is associated with small-cell BS s in time frame t, the out-of-cell interference received at the side of VU m, say $I^{\text{out}}_{sm,t}$, can be expressed as

$$I^{\text{out}}_{sm,t} = \sum_{s' \neq s, s' \in \mathcal{S}} g_{s'm,t} P_{s',t}. \tag{2}$$

We use $\hat{g}_{sm,t}$ to denote the real-time CSI of VU m when it is associated with small-cell BS s in time frame t, which is defined as

$$\tilde{g}_{sm,t} = \frac{g_{sm,t}}{I^{\text{out}}_{sm,t} + n_m} \tag{3}$$

with n_m being the noise power received at the user side. It is worth noting that every small-cell BS collects all CSI via the feedback from VUs, and thus the CSI of VU m obtained by small-cell BS s in time frame time t (denoted by $\hat{g}_{sm,t}$) would not be $\tilde{g}_{sm,t}$ due to the feedback delay. Specifically, suppose the feedback delay to be δ time frames, and $\hat{g}_{sm,t}$ can be expressed as

$$\hat{g}_{sm,t} = \tilde{g}_{sm,t-\delta}. \tag{4}$$

Clearly, we have $\delta = 0$ in the ideal V2S network where there is no feedback delay. Therefore, we start our work in the case where $\delta = 0$. As we know, the feedback delay would affect the cell association decision due to the out-of-date CSI, which will be studied in our future work. Let $\mathcal{U}_{s,t}$ denote the possible set of VUs associated with small-cell BS s in time frame t, where each VU selects small-cell BS s as a candidate of association station according to the strength of pilot signals from small-cell BS s. VU m adopts the SIC receiver to decode the data symbols from small-cell BS s to VU m, in which the interference-cancellation ordering of all VUs associated with small-cell BS s is in the increasing order of $\hat{g}_{sm,t}$'s for all $m \in \mathcal{U}_{s,t}$. On the other hand, the mobility of each VU is integrated into its channel states in each time frame by (1), and thus the transmission rate of VU m from small-cell BS s in time frame t is subject to $\boldsymbol{x}_{m,t}$'s. As a result, such transmission rate can be expressed as $r_{sm,t}(\boldsymbol{x}_{m,t}, \forall m)$, i.e.,

$$r_{sm,t}(\boldsymbol{x}_{m,t}, \forall m) = B \log \left(1 + \frac{p_{sm,t} \hat{g}_{sm,t}}{\sum\limits_{\forall m' \in \mathcal{U}_{s,t}: \hat{g}_{sm',t} > \hat{g}_{sm,t}} p_{sm',t} \hat{g}_{sm,t} + 1} \right) \tag{5}$$

in time frame t. Correspondingly, the total transmission rate of small-cell BS s, say $R_{s,t}(\boldsymbol{x}_{m,t}, \forall m)$, is equal to

$$R_{s,t}(\boldsymbol{x}_{m,t}, \forall m) = \sum_{\forall m \in \mathcal{U}_{s,t}} r_{sm,t}(\boldsymbol{x}_{m,t}, \forall m) \tag{6}$$

in time frame t. Since the long-term rate of small-cell BS s is subject to all $\{\boldsymbol{x}_{m,t}\}_{t=1,\cdots,\infty}$'s, and it can be expressed as

$$\bar{R}_s(\{\boldsymbol{x}_{m,t}\}_{t=1,\cdots,\infty}, \forall m) = \lim_{t\to\infty} \frac{1}{t} \sum_{\tau=1}^{t} R_{s,\tau}(\boldsymbol{x}_{m,\tau}, \forall m). \quad (7)$$

Correspondingly, the long-term achievable rate region $\mathcal{R}$ satisfies

$$\mathcal{R} = \left\{ \bar{\boldsymbol{R}} \middle| \bar{R}_s(\{\boldsymbol{x}_{m,t}\}_{t=1,\cdots,\infty}, \forall m) \right. \\ \text{subject to } 0 \le P_{s,t} \le P_{s,\max} \\ \left. \text{and } \sum_{\forall m \in \mathcal{U}_{s,t}} p_{sm,t} \le P_{s,t}, \forall s, t \right\}, \quad (8)$$

where $\bar{\boldsymbol{R}}$ is the vector of $\bar{R}_s(\cdot)$'s. Note that the set $\mathcal{R}$ corresponding to the set of all achievable rate vectors over long-term is shown to be a closed bounded convex set [29].

Considering the difference of small-cell BSs in service capacity due to the individual maximum transmit power, we formulate the criterion of load balancing as the function of $U_s(\bar{R}_s(\{\boldsymbol{x}_{m,t}\}_{t=1,\cdots,\infty}, \forall m))$ for small-cell BS s. Without losing generality, we assume that $U_s(\cdot)$ is an increasing, strictly concave and continuously differentiable utility function. Our target is to find the long-term rate vector $\bar{\boldsymbol{R}}$ corresponding to the long-term power control policy $\boldsymbol{p}_{sm} = (p_{sm,t}, \forall t = 1, \cdots)$ for all s and m that maximizes the network-wide aggregate utility across small-cell BSs over a long-term achievable rate region $\mathcal{R}$:

$$\mathbf{P}: \max_{\bar{\mathbf{R}}} \sum_{\forall \mathbf{s} \in \mathcal{S}} \mathbf{U_s}(\bar{\mathbf{R}}_\mathbf{s}(\{\boldsymbol{x}_{\mathbf{m,t}}\}_{\mathbf{t=1},\cdots,\infty}, \forall \mathbf{m})) \quad (9)$$

$$\text{s.t. } \bar{\boldsymbol{R}} \in \mathcal{R}. \quad (10)$$

Note that the decision of optimal long-term power control policy is dependent on the mobility process of each VU, and thus we need to take into account the VUs' mobility when designing the optimal policy.

Due to the convex nature of objective function and feasible set, Problem **P** is a convex optimization problem. Therefore, to find an optimal solution, we can use a standard gradient-based algorithm that selects the optimal power control maximizing the weighted sum rate with weights being marginal utilities in each time frame. In particular, for the optimal power control, we need to solve the following problem **P-control** in each time frame according to VUs' moving traces:

$$\mathbf{P-control}: \\ \max \sum_{\forall s \in \mathcal{S}} \underbrace{U_s'(\bar{R}_{s,t-1})}_{w_{s,t}} R_{s,t}(\boldsymbol{x}_{m,t}, \forall m) \\ \text{s. t. } 0 \le P_{s,t} \le P_{s,\max}, \quad \forall s \in \mathcal{S}, \\ \sum_{\forall m \in \mathcal{U}_{s,t}} p_{sm,t} \le P_{s,t}, \quad \forall s \in \mathcal{S} \\ \text{var. } P_{s,t}, p_{sm,t} \ge 0, \quad \forall s \in \mathcal{S}, \ \forall m \in \mathcal{M}. \quad (11)$$

Here, $U_s'(\cdot)$ is the first-order derivative of function $U_s(\cdot)$ over $\bar{R}_s(\{\boldsymbol{x}_{m,t}\}_{t=1,\cdots,\infty}, \forall m)$, and $\bar{R}_{s,t-1}$ is the long-term rate of small-cell BS s up to time frame t which satisfies $\bar{R}_{s,t} = \frac{1}{t}\sum_{\tau=1}^{t} R_{s,\tau}(\boldsymbol{x}_{m,\tau}, \forall m) = \bar{R}_{s,t-1} + \frac{1}{t}[R_{s,t}(\boldsymbol{x}_{m,t}, \forall m) - \bar{R}_{s,t-1}]$.

Note that the power control optimization problem in (11) is in general non-convex due to the mutual coupling among the out-of-cell interference of all VUs. Therefore, it is impossible to find the optimal solution based on the theory of convex optimization. It can be seen from (11) that there exist two types of power allocation: the power allocation corresponding to small-cell BSs and the power allocation corresponding to VUs. This motivates us to separately control the transmit power of small-cell BSs and VUs. Based on the system framework mentioned above, the optimal transmit power of small-cell BSs is determined at the station-centric controller, while the optimal transmit power of VUs is determined at the user-centric controller. In the following, we focus on designing the hierarchical power control algorithms performed at the station-centric and user-centric controllers, respectively.

IV. Hierarchical Power Control

Finding the optimization variables $P_{s,t}$ and $p_{sm,t}$ for all s and m in (11) is a non-convex optimization problem. Notably, given the power allocation of each small-cell BS, the user-centric controller of small-cell BS s can allocate the total power $P_s(t)$ to all associated VUs. In this section, we therefore want to solve the power control optimization problem in (11) in the following two stages. In the first stage, we present the power allocation algorithm performed at the user-centric controller of each small-cell BS to obtain the optimal power allocation among VUs associated with the same small-cell BS when the power allocation among small-cell BSs is given. In the second stage, according to the feedback of power allocation among VUs from the user-centric controller, the station-centric controller then determines the optimal power allocation among small-cell BSs. Before presenting the power control algorithm, we first derive some desirable properties of the optimal solution to problem (11).

A. Optimal Power Allocation at the User-Centric Controller

Note that given the total transmit power of each small-cell BS, problem (11) can be decomposed into multiple weighted sum rate maximization problems, each of which can be individually performed at the user-centric controller of each small-cell BS. By (6), the individual weighted sum rate maximization problem corresponding to small-cell BS s can be written as

$$\mathbf{IP}: \max \sum_{\forall \mathbf{m} \in \mathcal{U}_{\mathbf{s,t}}} \mathbf{r_{sm,t}}(\boldsymbol{x}_{\mathbf{m,t}}, \forall \mathbf{m}) \\ \text{s. t. } \sum_{\forall m \in \mathcal{U}_{s,t}} p_{sm,t} \le P_{s,t}, \\ \text{var. } p_{sm,t} \ge 0, \quad \forall m \in \mathcal{U}_{s,t}. \quad (12)$$

Next, the following proposition indicates the convex nature of the weighted sum rate maximization problem at the user-centric controller. The proof is given in Appendix A.

Lemma 1: Given the total transmit power of all small-cell BSs, the sum rate maximization problem in (12) can be transformed into a convex optimization problem.

Remark 1: The result in Proposition 1 can be extended to the general case where the objective function is a concave function of $r_{sm,t}(\cdot)$'s.

Lemma 1 reveals that the power allocation problem at the user-centric controller can be transformed into a convex optimization problem, and thus it can be solved by the convex optimization arguments. In the following, we present the optimal power allocation among all VUs associated with small-cell BS s (i.e., the optimal solution to problem (12)) when its total power $P_{s,t}$ is given. Based on the convex nature as shown in Lemma 1, Theorem 1 shows such optimal power allocation. The proof is given in Appendix B.

Theorem 1: To maximize the sum rate across VUs associated with small-cell BS s in time frame t (i.e., problem (12)), the total power of small-cell BS s should be greedily allocated to the VU with the best $\hat{g}_{sm,t}$.

By Theorem 1, the main operations at the user-centric controller is to first find the associated VU $m^*_{s,t}$ with the best $\hat{g}_{sm,t}$, i.e.,

$$\begin{aligned} m^*_{s,t} &= \underset{\forall m \in \mathcal{U}_{s,t}}{\text{argmax}} \quad \hat{g}_{sm,t} \\ &= \underset{\forall m \in \mathcal{U}_{s,t}}{\text{argmax}} \quad \frac{g_{sm,t}}{\sum\limits_{\forall s' \neq s, s' \in \mathcal{S}} g_{s'm,t} P_{s',t} + n_m}, \end{aligned} \tag{13}$$

and then to allocate the total transmit power $P_{s,t}$ to the associated VU $m^*_{s,t}$.

B. Optimal Power Allocation at the Station-Centric Controller

In this subsection, we present the optimal power allocation among all small-cell BSs at the station-centric controller.

By Theorem 1, the optimal power allocation problem at the station-centric controller can be rewritten as

$$\begin{aligned} \mathbf{SP}: \\ &\max \sum_{\forall s \in \mathcal{S}} w_{s,t} B \log\left(1 + \max_{\forall m \in \mathcal{U}_{s,t}} \frac{P_{s,t} g_{sm,t}}{\sum\limits_{\forall s' \neq s, s' \in \mathcal{S}} g_{s'm,t} P_{s',t} + n_m}\right) \\ &\text{s. t. } 0 \le P_{s,t} \le P_{s,\max}, \forall s \in \mathcal{S}, \\ &\text{var. } P_{s,t}, \forall s \in \mathcal{S}. \end{aligned} \tag{14}$$

in each time frame t.

The following Theorem states the property of the optimal solution to problem (14) (and hence problem (11)). The proof is given in Appendix C.

Theorem 2: One small-cell BS at least, say small-cell BS s, transmits information with its maximum allowable transmit power $P_{s,\max}$ when maximizing the weighted sum rate in (11).

Note that the objective function in problem (14) is monotonically increasing with the increase of each SINR term $\frac{P_{s,t} g_{sm,t}}{\sum\limits_{\forall s' \neq s, s' \in \mathcal{S}} g_{s'm,t} P_{s',t} + n_m}$, and thus we can obtain the optimal solution to problem (14) based on the theory of monotonic optimization [31]. However, due to the complicated interference coupling between small-cell BSs, it requires exponential computational complexity though the global optimal solution is obtained based on the idea of monotonic optimization. This implies that from the implementation perspective, it is intractable to obtain the global optimal solution in each time frame. Therefore, it is of practical meaning to design a low-complexity near-optimal algorithm for the station-centric controller.

For the low-complexity solution, we want to solve problem (14) based on the idea of successive convex approximation. In particular, there are three key ingredients at each iteration l as follows.

1) Form the k-th approximated problem of (14) based on the approximation around the solution $\boldsymbol{P}_t^{(l-1)} = (P_{1,t}^{(l-1)}, \cdots, P_{S,t}^{(l-1)})$ obtained at the $(l-1)$-th iteration.
2) Solve the l-th approximated problem to obtain $\boldsymbol{P}_t^{(l)}$.
3) Increment l and go to step 1 until convergence to a stationary point.

In the following, we shall introduce every key ingredient in details. In particular, the proposed algorithm works as follows.

First, we choose an initial feasible point $\boldsymbol{P}_t^{(0)}$ to start algorithm. By [32, Lemma 1], problem (14) can be approximated as

$$\begin{aligned} &\max \sum_{\forall s \in \mathcal{S}} w_{s,t} B \beta_s^{(l)} \log \frac{P_{s,t} g_{sm^{*(l)}_{s,t},t} / \beta_s^{(l)}}{\sum\limits_{\forall s' \neq s, s' \in \mathcal{S}} g_{s'm^{*(l)}_{s,t},t} P_{s',t} + n_{m^{*(l)}_{s,t}}} \\ &\quad + w_{s,t} B \alpha_s^{(l)} \\ &\text{s. t. } 0 \le P_{s,t} \le P_{s,\max}, \quad \forall s \in \mathcal{S}, \\ &\text{var. } P_{s,t}, \forall s \in \mathcal{S} \end{aligned} \tag{15}$$

at the l-th iteration. Here, $m^{*(l)}_{s,t}$ is obtained by (13) with $P_{s,t} = P_{s,t}^{(l-1)}$ for all s, and $\alpha_s^{(l)}$ and $\beta_s^{(l)}$ are respectively calculated as

$$\begin{aligned} \alpha_s^{(l)} = &\frac{\sum\limits_{\forall s' \neq s, s' \in \mathcal{S}} g_{s'm^{*(l)}_{s,t},t} P_{s',t}^{(l-1)} + n_{m^{*(l)}_{s,t}}}{\sum\limits_{\forall s' \in \mathcal{S}} g_{s'm^{*(l)}_{s,t},t} P_{s',t}^{(l-1)} + n_{m^{*(l)}_{s,t}}} \\ &\times \log \frac{\sum\limits_{\forall s' \in \mathcal{S}} g_{s'm^{*(l)}_{s,t},t} P_{s',t}^{(l-1)} + n_{m^{*(l)}_{s,t}}}{\sum\limits_{\forall s' \neq s, s' \in \mathcal{S}} g_{s'm^{*(l)}_{s,t},t} P_{s',t}^{(l-1)} + n_{m^{*(l)}_{s,t}}} \end{aligned} \tag{16}$$

and

$$\beta_s^{(l)} = \frac{P_{s,t}^{(l-1)} g_{sm^{*(l)}_{s,t},t}}{\sum\limits_{\forall s' \in \mathcal{S}} g_{s'm^{*(l)}_{s,t},t} P_{s',t}^{(l-1)} + n_{m^{*(l)}_{s,t}}}. \tag{17}$$

Second, we focus on solving problem (15). For the notational brevity, we use $u_s(P_{s,t}, \boldsymbol{P}_{-s,t})$ to denote $w_{s,t} B(\alpha_s^{(l)} + \beta_s^{(l)} \log \frac{P_{s,t} g_{sm^{*(l)}_{s,t},t} / \beta_s^{(l)}}{\sum\limits_{\forall s' \neq s, s' \in \mathcal{S}} g_{s'm^{*(l)}_{s,t},t} P_{s',t} + n_{m^{*(l)}_{s,t}}})$, where $\boldsymbol{P}_{-s,t} = (P_{1,t}, \cdots, P_{s-1,t}, P_{s+1,t}, \cdots, P_{S,t})$. Based on the key idea of best-response pricing algorithm [33], the optimal solution to problem (15) can be obtained by iteratively solving S optimization problems in parallel:

$$\begin{aligned} &\max_{P_{s,t}} u_s(P_{s,t}, \boldsymbol{P}^-_{-s,t}) - \pi_s(\boldsymbol{P}_t^-) P_{s,t} \\ &\text{s. t. } 0 \le P_{s,t} \le P_{s,\max}, \quad \forall s \in \mathcal{S}, \end{aligned} \tag{18}$$

where $\boldsymbol{P}_t^-$ means the vector of $P_{s,t}^-$'s obtained at the previous iteration. and the price $\pi_s(\boldsymbol{P}_t^-)$ satisfies

$$\pi_s(\boldsymbol{P}_t^-) = \sum_{\forall s' \neq s, s' \in \mathcal{S}} \frac{w_{s',t} B \beta_{s'}^{(l)} g_{s m_{s',t}^{*(l)},t}}{\sum_{\forall \hat{s} \neq s', \hat{s} \in \mathcal{S}} g_{\hat{s} m_{s',t}^{*(l)},t} P_{\hat{s},t}^- + n_{m_{s',t}^{*(l)}}}. \quad (19)$$

Since the function $u_s(P_{s,t}, \boldsymbol{P}_{-s,t}^-) - \pi_s(\boldsymbol{P}_t^-)P_{s,t}$ is concave in $P_{s,t}$, the optimal solution to problem (18), say $\hat{P}_{s,t}$, is uniquely calculated as

$$\hat{P}_{s,t} = \min\{\frac{w_{s,t} B \beta_s^{(l)}}{\pi_s(\boldsymbol{P}_t^-)}, P_{s,\max}\}. \quad (20)$$

In summary, the optimal solution to problem (15) can be obtained by Procedure 1. Furthermore, the following Theorem 3 shows that Procedure 1 globally converges to the optimal solution to problem (15). The proof is given in Appendix D.

Theorem 3: Procedure 1 can globally converge to the optimal solution to problem (15).

Third, we can repeat the procedure above until convergence to a stationary point of problem (14). In particular, the algorithm terminates at the kth iteration if $||\boldsymbol{P}_t^{(l)} - \boldsymbol{P}_t^{(l-1)}|| \leq \epsilon$, where ϵ is the error tolerance for exit condition.

Having introduced the basis operations, we now formally present the low-complexity power control algorithm operated at the station-centric controller as Algorithm 1. Furthermore, the following Theorem 4 shows the convergence property of the proposed power control algorithm. The proof is given in Appendix E.

Theorem 4: In the proposed power control algorithm, the solutions of this series of approximations (15) converge to a point satisfying the necessary KKT optimality conditions of problem (14).

Procedure 1 Achieve the Optimal Solution to Problem (15)

1: Let $(\hat{P}_{1,t}, \cdots, \hat{P}_{S,t}) = \boldsymbol{P}_t^{(l-1)}$.
2: **repeat**
3: Let $P_{s,t}^- = \hat{P}_{s,t}$ for all s.
4: Obtain $\hat{P}_{s,t}$ for all s by (19)-(20).
5: **until** $\max_{\forall s \in \mathcal{S}} |\hat{P}_{s,t} - P_{s,t}^-| \leq \delta$, where δ is a small positive constant as a termination criterion.
6: Output: $\boldsymbol{P}_t^{(l)} = \boldsymbol{P}_t^-$.

V. Simulation Results

In this section, we conduct simulations to illustrate the effectiveness of the proposed power control algorithm. Following the networking parameters suggested in [35], we set the simulation parameters in Table I. We use Clarke's model [36] to generate the fading level, and the coherence time of channel fading is larger than 4 ms due to the fact that maximum VU velocity is 60 km/h. Suppose that the changes in the fading level occur relatively slowly during one time frame, and thus we set the length of time frame to be 1 ms, which implies the station-centric controller and user-centric controllers are allowed to dynamically update the VU association via power control per millisecond.[1]

Algorithm 1 The Low-Complexity Power Control Algorithm at the Station-Centric Controller

1: **Initialization:** Randomly choose an initial feasible point $\boldsymbol{P}_t^{(0)}$, and let $l = 0$.
2: **repeat**
3: Set $l = l + 1$.
4: Update $m_{s,t}^{*(l)}$'s, $\alpha_s^{(l)}$'s, and $\beta_s^{(l)}$ with $\boldsymbol{P}^{(l-1)}$'s by (13), (16), and (17), respectively.
5: Approximate problem (14) as problem (15) with $m_{s,t}^{*(l)}$'s, $\alpha_s^{(l)}$'s, and $\beta_s^{(l)}$'s.
6: Obtain $\boldsymbol{P}^{(l)}$ by solving problem (15) via Procedure 1.
7: **until** $||\boldsymbol{P}_t^{(l-1)} - \boldsymbol{P}_t^{(l)}|| \leq \epsilon$.
8: Output: $\boldsymbol{P}^{(l)}$ as the optimal power allocation among all small-cell stations.

TABLE I
Simulation Parameters

Simulation parameters	Value choice
Carrier frequency	2000MHz
Bandwidth	20MHz
Path loss model	$(128.1 + 37.6\log_{10}(d))$dB ($d$ in km)
Fading model	Rayleigh fading
Noise power spectral density	-174dBm/Hz
Range of maximum transmit power $P_{s,\max}$	250mW $\sim$ 2W
Small-cell Radius	100m $\sim$ 300m
Maximum VU velocity	60km/h
Time frame length	1 ms

A. Global Optimality and Computational Complexity

Example 1: In this simulation example, we want to verify the optimality and computational complexity of the proposed power control algorithm operated at the station-centric controller for the downlink NOMA-enabled V2S network as shown in Fig. 3(a) at a certain time frame. Specifically, we consider a circle-road scenario with four two-direction lanes, in which ten small-cell BSs are uniformly deployed along with the 400-meter/420-meter two-dimensional inner/outer circle planes and M VUs are randomly moving on the four lanes. We assume that the weight w_s is uniformly chosen in [0,1]. Also, we set the maximum allowable transmit power and cell radiuses of ten small-cell BSs to be (0.25 1.5 0.25 1.0 1.25 1.75 1.5 1.25 0.75 1.5)W and (125 250 125 200 225 275 250 225 175 250)m, respectively.

Fig. 4 illustrates the convergence and optimality of the proposed algorithm with the error tolerance $\epsilon = 10^{-9}$ when

[1]The station-centric controller informs user-centric controllers of transmit power via fiber, whose latency is equal to 5μs per kilometer [37]. On the other hand, the computing takes can be realized in the station-centric controller and user-centric controllers through equipping them with cloud computing servers, which can guarantee the computing delay at the order of millisecond [38] Therefore, the dynamic updating can be performed per millisecond.

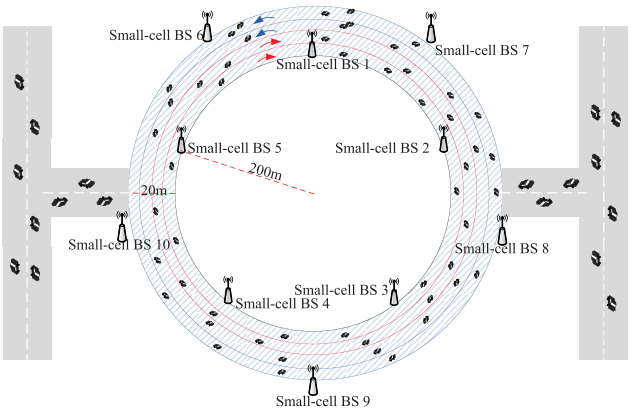

(a) Circle-road scenario

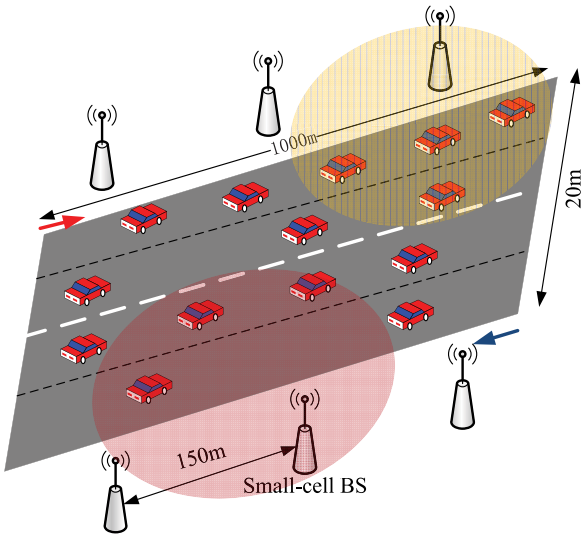

(b) Linear-road scenario

Fig. 3. NOMA-enabled V2S network topologies.

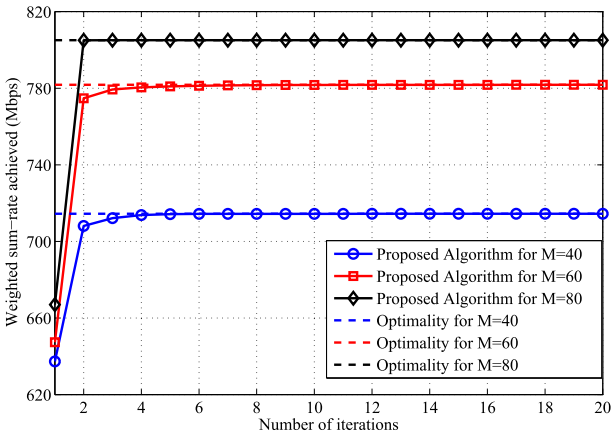

Fig. 4. Convergence and optimality of weighted sum-rate for the proposed power control algorithm.

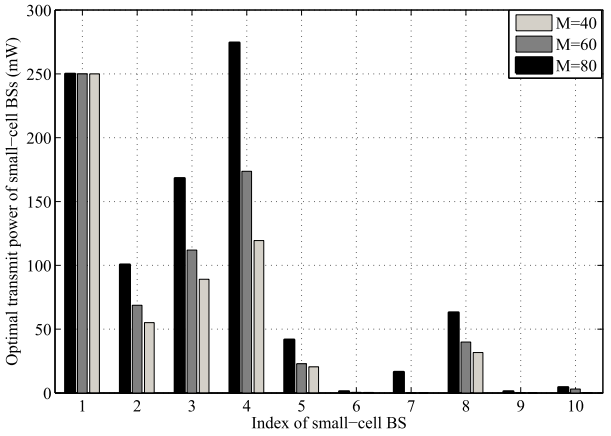

Fig. 5. Optimal power allocation of ten small-cell BSs in Fig. 3(a).

varying the number of VUs. For the comparison, we also obtain the optimal weighted sum-rate on the framework of monotonic optimization. As shown in Fig. 4, the convergence of the proposed algorithm is fast, with the obtained weighted sum-rate very close to the optimal weighted sum-rate by less than 20 iterations. This observation implies that the millisecond-order time scale of updating VU association is acceptable for the V2S network. We can further find that the obtained weighted sum-rate increases with the increase of the number of VUs. This is because that each small-cell BS is more likely to associate with VUs with good channel conditions with increasing the number of VUs.

Fig. 5 shows the optimal power allocation of ten small-cell BSs under the different density of VUs. We can find that at least one small-cell BS (i.e., small-cell BS 1) serves its associated VU with the maximum allowable transmit power, which coincides with the result in Theorem 2. Furthermore, it can be seen that the number of off small cells is increasing with the increase of the number of VUs. This is mainly because that the co-channel interference can severely affect the weighted sum-rate of V2S network. In particular, the co-channel interference among small-cells becomes severer in the denser population of VUs, and thus the weighted sum-rate can be improved by turning off some small-cells that are experiencing severe the co-channel interference.

B. Performance Comparison

To the best of our knowledge, there are no algorithms proposed with the same goal in the literature. For the comparison with our proposed power control based VU association scheme, we therefore introduce two baseline schemes: maximum-power based random association scheme and maximum-power based best VU association scheme. The maximum-power based random association scheme assumes that in each time frame, every small-cell BS randomly serves one VU in its footprint with the maximum transmit power. The maximum-power based best VU association scheme assumes that in each time frame, every small-cell BS s serves the VU with the best $\hat{g}_{sm,t}$ using the maximum transmit power. We evaluate the system performance in terms of long-term system utility, total energy consumption across small-cell BSs, and service time. Here, the service time means the total time that each VU is associated to one small-cell BS, which is averaged on all VUs during the simulation time. Therefore, the service time can be used to evaluate the handover rate of the proposed scheme, and the more service time implies the less handover rate..

Example 2: In this simulation example, we want to compare the proposed scheme with the maximum-power based random association scheme (Scheme 1 for simplification) and the maximum-power based best VU association scheme (Scheme 2 for simplification) when they are applied to the NOMA-enabled V2S network in Fig. 3(a). We assume that a fixed number of VUs are uniformly moving on the four two-direction lanes for sixty thousand of time frames (i.e., 60s), and we vary the number of VUs from 40 to 80.

Fig. 6 shows the system performance obtained in different VU densities when the proportional fairness (i.e., $U_s(\bar{R}_s(\cdot)) = \log \bar{R}_s(\cdot)$) is used as the load balancing criterion. Fig. 7 shows the system performance obtained in different VU densities when the weighted sum rate across small-cell BSs (i.e., $U_s(\bar{R}_s(\cdot)) = w_s \bar{R}_s(\cdot)$) is used as the load balancing criterion, where we set the weight w_s to be uniformly chosen in [0,1] for all s. From Figs. 6 and 7, we find that with increasing the number of VUs, the long-term system-wide utility slowly increases, while the service time and total energy consumption decreases when applying the proposed scheme. Since the VUs served by small-cell BSs have the better channel conditions with the increase of the number of VUs, the long-term system-wide utility increases and less total energy consumption is needed for interference mitigation accordingly. Since the proposed scheme associates the VU to the small-cell BS according to the max-SINR policy, the association probability of each VU becomes lower with the increase of the number of VUs, which leads to the decreasing of service time. We further find that the proposed scheme always outperforms the two baseline schemes in terms of long-term system-wide utility, total energy consumption across small-cell BSs, and service time. In particular, the proposed scheme can improve the long-term system-wide performance with lower energy consumption, which implies more spectral and energy efficiency. On the other hand, the proposed scheme can guarantee the longer service time on average, which implies infrequent handover rate.

Example 3: In this simulation example, we want to compare the proposed scheme with the maximum-power based random association scheme (Scheme 1) and the maximum-power based best VU association scheme (Scheme 2) when they are applied to the NOMA-enabled V2S network in Fig. 3(b). Specifically, twelve small-cell BSs are uniformly distributed along with two sides of 1000m-linear-road, in which the distance between any two neighboring small-cell BSs at the same side is 150m. A dynamic number of VUs are moving on the four two-direction lanes for one hundred thousand of time frames (i.e., 100s). The arriving model of VUs is assumed to be a Poisson Process with the arriving rate being λ VUs per second at each direction, and each arriving VU is assumed to uniformly select a lane.

Fig. 8 shows the system performance obtained with the different arriving rate of VUs when the proportional fairness (i.e., $U_s(\bar{R}_s(\cdot)) = \log \bar{R}_s(\cdot)$) is used as the load balancing criterion. Fig. 9 shows the system performance obtained with the different arriving rate of VUs when the weighted sum rate across small-cell BSs (i.e., $U_s(\bar{R}_s(\cdot)) = w_s \bar{R}_s(\cdot)$) is used as the load balancing criterion, where we set the weight w_s to be uniformly chosen in [0,1] for all s. From Figs. 8 and 9, we can find that with the increase of the arriving rate of VUs, the total energy consumption and service time decrease, while the long-term system-wide utility increases. The main reason is that the increase of the arriving rate of VUs leads to

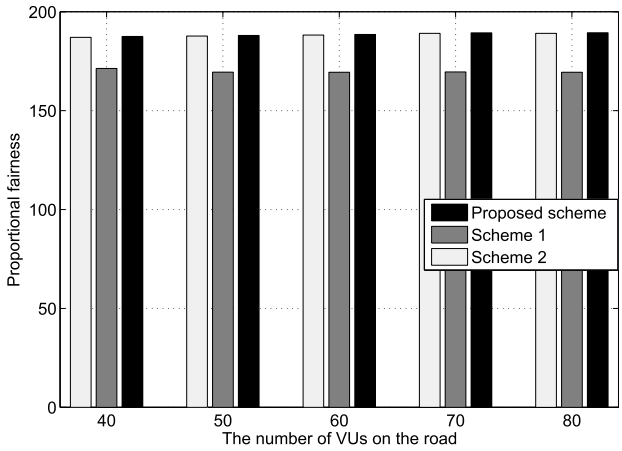

(a) Proportional fairness

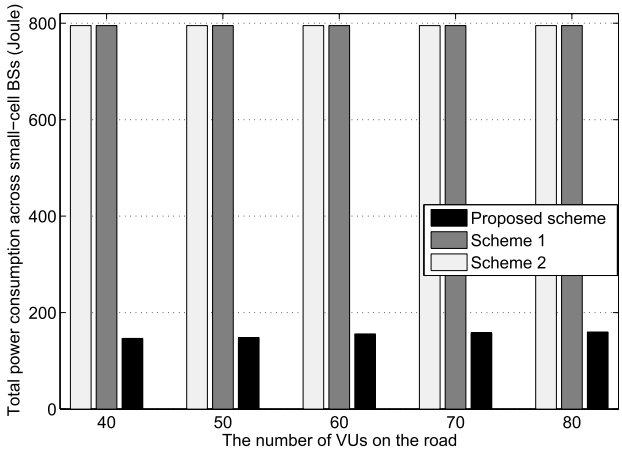

(b) Total energy consumption

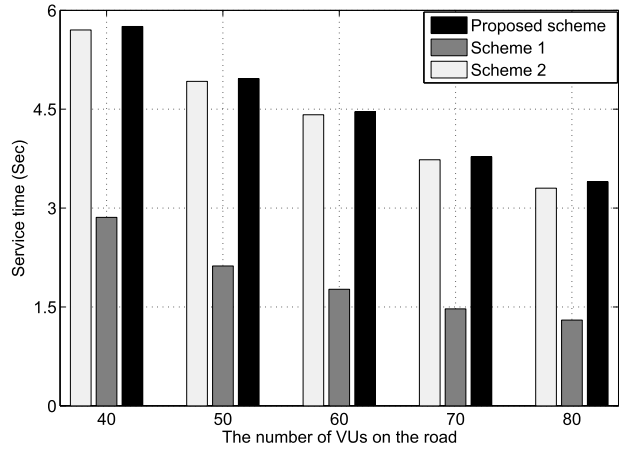

(c) Service time

Fig. 6. The system performance obtained when the proportional fairness utility is considered for the scenario in Fig. 3(a).

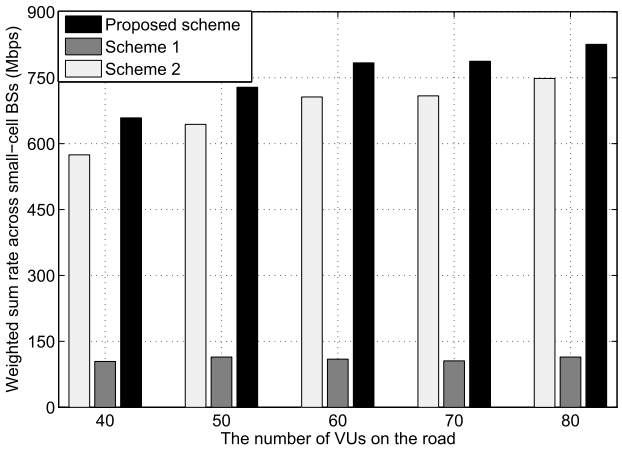

(a) Weighted sum rate maximization

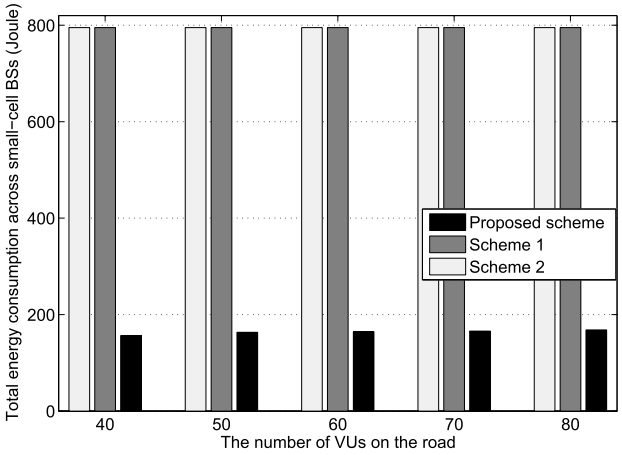

(b) Total energy consumption

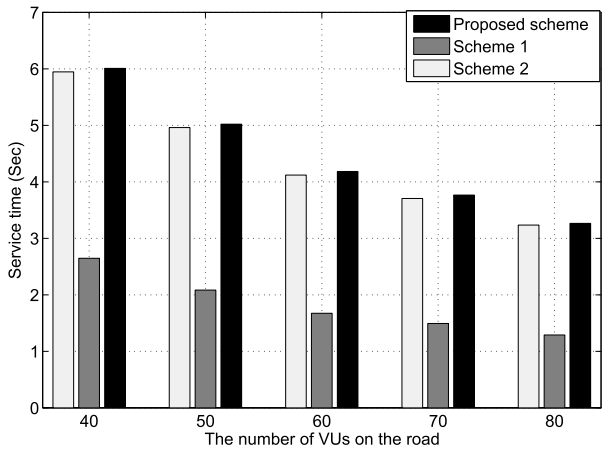

(c) Service time

Fig. 7. The performance of individual VUs obtained when the weighted sum-rate utility is considered for the scenario in Fig. 3(a).

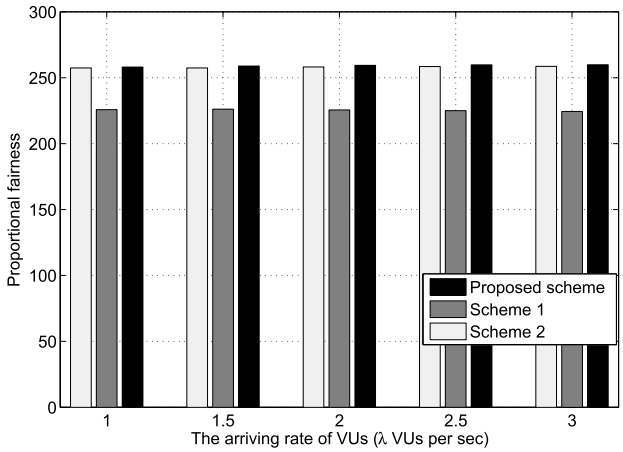

(a) Proportional fairness

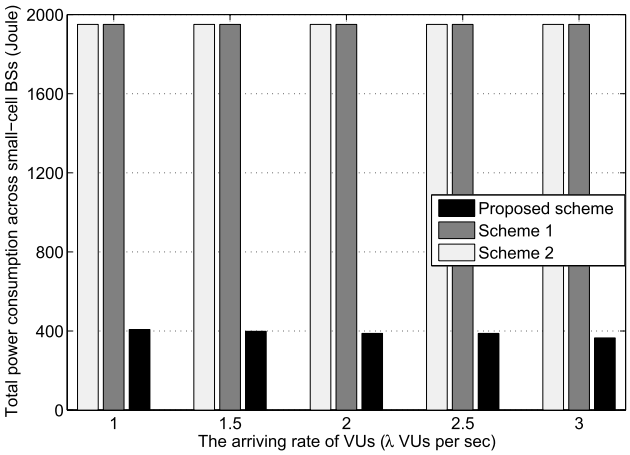

(b) Total energy consumption

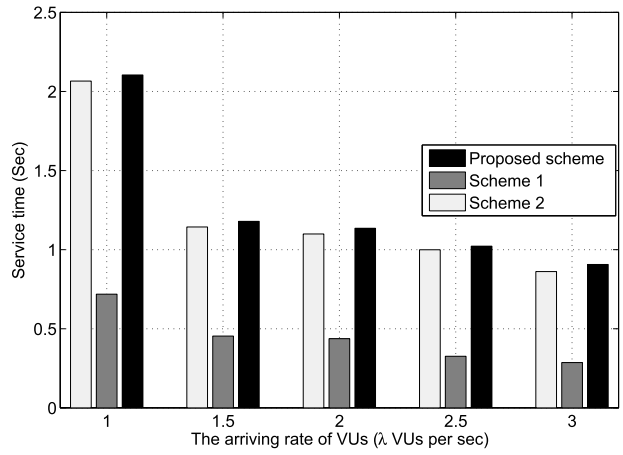

(c) Service time

Fig. 8. The system performance obtained when the weighted sum-rate utility is considered for the scenario in Fig. 3(b).

more VUs moving on the road, and thus each small-cell BS is more likely to serve VUs with the better channel conditions. Also, we can find that the proposed scheme always outperforms the two baseline schemes when they are applied to the linear-road scenario. This is mainly because that the hierarchical power control is adopted in the proposed scheme to adaptively adjust the cell association and power control for every small-cell BS according to the time-varying traffic load and communication environments due to the vehicle mobility. The observation implies that compared to the two baseline

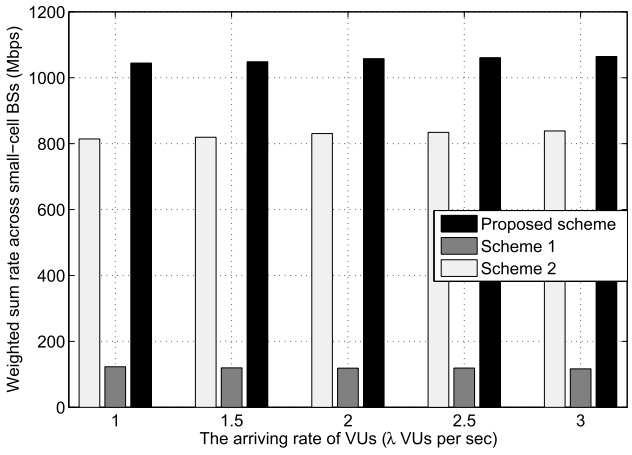

(a) Weighted sum rate maximization

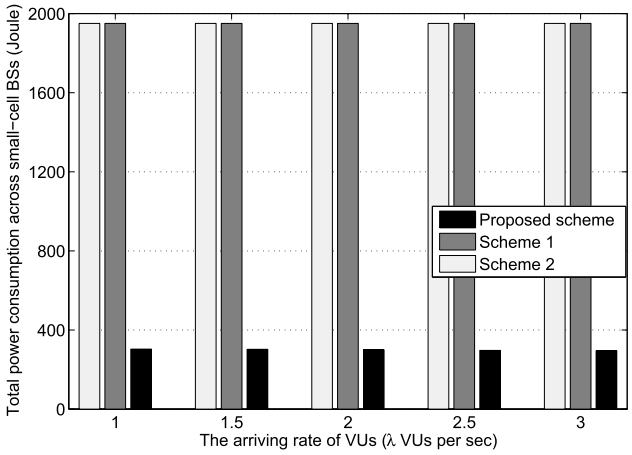

(b) Total energy consumption

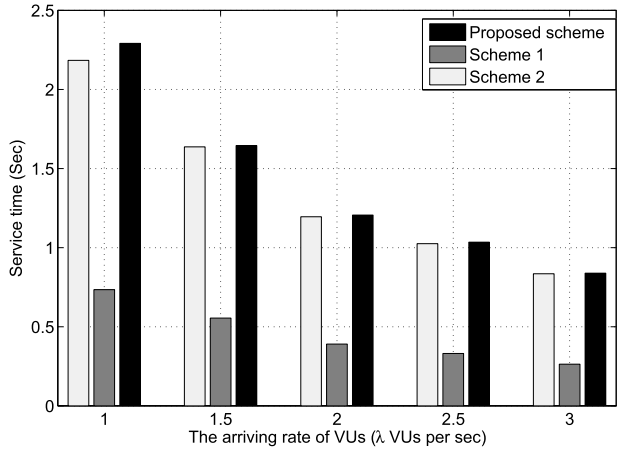

(c) Service time

Fig. 9. The performance of individual VUs obtained when the weighted sum-rate utility is considered for the scenario in Fig. 3(b).

schemes, the proposed scheme has more spectrum and energy efficiency and less handover.

Furthermore, we have to note that in both circle-road scenario and linear road scenario, the maximum-power based best VU association scheme can achieve the similar long-term

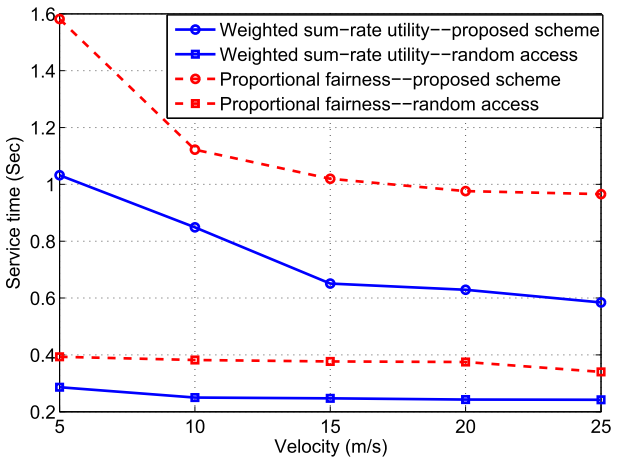

Fig. 10. The service time versus the velocity.

system-wide utility at the cost of more energy consumption in comparison with the proposed scheme. This implies that if the spectral efficiency is the main goal, the cell association is sufficient without power control for V2S networks.

Example 4: In this simulation example, we want to evaluate the influence of vehicle velocity when applying the proposed scheme to the V2S network in Fig. 3(b). We set the arriving rate to be 2 VUs per second at each direction, and other settings are the same as those in Example 3. Fig. 10 illustrates the service time obtained with the different vehicle velocity when maximizing either the proportional fairness or the weighted sum-rate utility. For the comparison purpose, we also plot the service time obtained when the random access technique is applied to such a V2S network. From Fig. 10, we can see that the service time obtained by the proposed scheme is decreasing with the increase of velocity for the proportional fairness utility and the weighted sum-rate utility. Further, compared to adopting the the weighted sum-rate utility, VUs can obtain more service time when adopting the proportional fairness utility. Also, it can be seen from Fig. 10 that the proposed scheme always outperforms the random access technique.

VI. Conclusions

In this paper, we have studied the joint optimization of cell association and power control that maximizes the long-term system utility to enhance the long-term system-wide performance and avoid excessive handovers for NOMA-enabled V2S networks. Specifically, we first transform such a joint optimization problem into a weighted sum rate maximization problem in each time frame based on a standard gradient-based algorithm. Then, the equivalent weighted sum rate maximization problem is efficiently solved by the proposed hierarchical power control algorithm which performs the optimal power allocation for small-cell BSs and VUs in the station-centric decision layer and the user-centric decision layer, respectively. By comparing with the proposed algorithm, we have gained deeper understanding of the baseline schemes: the maximum-power based random association scheme and the maximum-power based best VU association scheme. Simulations further show that the proposed algorithm performs better performance

in terms of spectrum-energy efficiency and handover rate for the joint optimization of cell association and power control.

For our future work, the predication on the mobility of VUs and the feedback delay of CSI will be taken into account when designing the joint cell association and power control for NOMA-enabled V2S networks. Furthermore, the emerging 5G techniques, such as massive MIMO, mmWave communication, and full-duplex communication, will be applied to V2S networks to further improve the spectral and energy efficiency and reduce the handover rate.

APPENDIX

A. Proof of Lemma 1

For the notational brevity, we sort all users associated with small-cell BS s in the descending order of $\hat{g}_{sm,t}$'s, use $m_s(k)$ to denote the user index in the kth position in the sorted sequence, and abbreviate $r_{sm,t}(\boldsymbol{x}_{m,t}, \forall m)$ into $r_{sm,t}$. Therefore, the data rate $r_{sm_s(k),t}$ in (5) can be rewritten as

$$2^{\frac{r_{sm_s(k),t}}{B}} = 1 + \frac{p_{sm_s(k),t}}{\sum_{j=1}^{k-1} p_{sm_s(j),t} + 1/\hat{g}_{sm_s(k),t}}, \quad \forall k \in \{1, \cdots, |\mathcal{U}_{s,t}|\}, \tag{21}$$

where $|\mathcal{U}_{s,t}|$ means the cardinality of $\mathcal{U}_{s,t}$. Since the data rate $r_{sm_s(k),t}$ increases with the transmit power, the power constraint in (12) is active when the optimal solution to problem (12) is obtained. Therefore, by solving a set of equations in (21) and $\sum_{k=1}^{|\mathcal{U}_{s,t}|} p_{sm_s(k),t} = P_{s,t}$, we have

$$\sum_{k=1}^{|\mathcal{U}_{s,t}|} \exp\left(\frac{\ln 2}{B} \sum_{i=k}^{|\mathcal{U}_{s,t}|} r_{sm_s(i),t}\right)\left(\frac{1}{\hat{g}_{sm_s(k),t}} - \frac{1}{\hat{g}_{sm_s(k-1),t}}\right) = P_{s,t} + \frac{1}{\hat{g}_{sm_s(|\mathcal{U}_{s,t}|),t}}. \tag{22}$$

Since the objective function in (12) is an increasing function of $r_{sm_s(k),t}$'s, it follows from (22) that problem (12) can be rewritten as

$$\begin{aligned} \textbf{IPN}: \quad & \max \quad \sum_{k=1}^{|\mathcal{U}_{s,t}|} r_{sm_s(k),t} \\ & \text{s. t.} \quad \sum_{k=1}^{|\mathcal{U}_{s,t}|} \exp\left(\frac{\ln 2}{B} \sum_{i=k}^{|\mathcal{U}_{s,t}|} r_{sm_s(i),t}\right)\left(\frac{1}{\hat{g}_{sm_s(k),t}} - \frac{1}{\hat{g}_{sm_s(k-1),t}}\right) \\ & \qquad \le P_{s,t} + \frac{1}{\hat{g}_{sm_s(|\mathcal{U}_{s,t}|),t}}, \\ & \text{var. } r_{sm_s(k),t} \ge 0, \forall k = 1, \cdots, |\mathcal{U}_{s,t}|. \end{aligned} \tag{23}$$

Due to the fact that $\frac{1}{\hat{g}_{sm_s(k),t}} - \frac{1}{\hat{g}_{sm_s(k-1),t}}$ is non-negative for all k, the constraint in (23) is convex [30]. Together with a linear objective function, it follows that problem (23) is a convex optimization problem. Therefore, Proposition 2 follows. ■

B. Proof of Theorem 1

For the notational brevity, we abbreviate $r_{sm,t}(\boldsymbol{x}_{m,t}, \forall m)$ into $r_{sm,t}$. By Lemma 1, the optimal solution to problem (12) can be obtained by solving the convex optimization problem (23). Due to the convex nature, we can obtain the optimal solution to problem (23) based on the KKT conditions (24):

$$\begin{aligned} & J(\{r_{sm_s(k),t}\}, \lambda, \{\mu_k\}) \\ & = \sum_{k=1}^{|\mathcal{U}_{s,t}|} r_{sm_s(k),t} + \sum_{k=1}^{|\mathcal{U}_{s,t}|} \mu_k r_{sm_s(k),t} \\ & \quad + \lambda\Bigg(P_{s,t} + \frac{1}{\hat{g}_{sm_s(|\mathcal{U}_{s,t}|),t}} \\ & \quad - \sum_{k=1}^{|\mathcal{U}_{s,t}|} \exp\left(\frac{\ln 2}{B} \sum_{i=k}^{|\mathcal{U}_{s,t}|} r_{sm_s(i),t}\right)\left(\frac{1}{\hat{g}_{sm_s(k),t}} - \frac{1}{\hat{g}_{sm_s(k-1),t}}\right)\Bigg), \end{aligned} \tag{24}$$

where λ and μ_k are the Lagrange multipliers for the first constraint in (23) and the constraint of $r_{sm_s(k),t} \ge 0$, respectively. Since the objective function and the constraint function in (23) are both increasing with $r_{sm_s(k),t}$'s, the optimal solution to problem (23) is obtained only when the first constraint of (23) is active. Therefore, applying the KKT conditions, the optimal solution to problem (23) corresponds to the solution to the following equations:

$$\begin{aligned} \frac{\partial J(\cdot)}{\partial r_{sm_s(k),t}} &= 1 + \mu_k - \frac{\mu \ln 2}{B} \\ &\quad \times \sum_{i=1}^{k} \exp\left(\frac{\ln 2}{B} \sum_{j=i}^{|\mathcal{U}_{s,t}|} r_{sm_s(j),t}\right) \\ &\quad \times \left(\frac{1}{\hat{g}_{sm_s(i),t}} - \frac{1}{\hat{g}_{sm_s(i-1),t}}\right) \\ &= 0, \forall k, \\ &\quad \sum_{k=1}^{|\mathcal{U}_{s,t}|} \exp\left(\frac{\ln 2}{B} \sum_{i=k}^{|\mathcal{U}_{s,t}|} r_{sm_s(i),t}\right) \\ &\quad \times \left(\frac{1}{\hat{g}_{sm_s(k),t}} - \frac{1}{\hat{g}_{sm_s(k-1),t}}\right) \\ &= P_{s,t} + \frac{1}{\hat{g}_{sm_s(|\mathcal{U}_{s,t}|),t}}, \\ \mu_k r_{sm_s(k),t} &= 0, \quad \mu_k \ge 0, \ \forall k, \lambda > 0. \end{aligned} \tag{25}$$

From (25), we have

$$\begin{aligned} \frac{\partial J(\cdot)}{\partial r_{sm_s(k+1),t}} &= \mu_{k+1} - \mu_k \\ &\quad - \exp\left(\frac{\ln 2}{B} \sum_{i=k+1}^{|\mathcal{U}_{s,t}|} r_{sm_s(i),t}\right) \\ &\quad \times \left(\frac{1}{\hat{g}_{sm_s(k+1),t}} - \frac{1}{\hat{g}_{sm_s(k),t}}\right) = 0. \end{aligned} \tag{26}$$

Due to the fact that $\exp\left(\frac{\ln 2}{B} \sum_{i=k+1}^{|\mathcal{U}_{s,t}|} r_{sm_s(i),t}\right)\left(\frac{1}{\hat{g}_{sm_s(k+1),t}} - \frac{1}{\hat{g}_{sm_s(k),t}}\right) > 0$, it follows from (26) that $\mu_1 = 0$ and $\mu_k > 0$

for all $k > 1$. By (25), this implies that the optimal solution to problem (23) (and hence problem (12)) is obtained when small-cell BS s only serves the user $m_s(1)$ with all power $P_{s,t}$. Therefore, Theorem 1 follows. ■

C. Proof of Theorem 2

Assume two power allocation vectors $\boldsymbol{P}_{1,t}$ and $\boldsymbol{P}_{2,t}$ in time frame t such that $\boldsymbol{P}_{1,t} = [P_{11,t}, \cdots, P_{1S,t}] \prec [P_{1,\max}, \cdots, P_{S,\max}]$ and $\boldsymbol{P}_{2,t} = \kappa \boldsymbol{P}_{1,t}$ with $\kappa = \min_s \frac{P_{s,\max}}{P_{1s,t}} > 1$. It is obvious that $\max_{\forall m \in \mathcal{U}_{s,t}} \{P_{2s,t} g_{sm,t} / (\sum_{\forall s' \neq s, s' \in \mathcal{S}} g_{s'm,t} P_{2s',t} + n_m)\} = \max_{\forall m \in \mathcal{U}_{s,t}} \{P_{1s,t} g_{sm,t} / (\sum_{\forall s' \neq s, s' \in \mathcal{S}} g_{s'm,t} P_{1s',t} + n_m/\kappa)\} > \max_{\forall m \in \mathcal{U}_{s,t}} \{P_{1s,t} g_{sm,t} / (\sum_{\forall s' \neq s, s' \in \mathcal{S}} g_{s'm,t} P_{1s',t} + n_m)\}$ for all s due to the fact that $\kappa > 1$. It follows that that the weighted sum rate in (14) corresponding to $\boldsymbol{P}_{2,t}$ is larger than that corresponding to $\boldsymbol{P}_{1,t}$, since it is increasing with the maximum SINR achieved by each small-cell BS. This implies that the optimal power allocation of small-cell BSs in problem (14) must contain at least one element equal to $P_{s,\max}$. Since problem (14) is equivalent to problem (11), Theorem 2 follows. ■

D. Proof of Theorem 3

We denote the term $\frac{P_{s,t} g_{sm_{s,t}^{*(k)},t} / \beta_s^{(k)}}{\sum_{\forall s' \neq s, s' \in \mathcal{S}} g_{s'm_{s,t}^{*(k)},t} P_{s',t} + n_{m_{s,t}^{*(k)}}}$ as γ_s. Over the transformed variables $\tilde{P}_{s,t} = \log P_{s,t}$ and $\tilde{\gamma}_s = \log \gamma_s$ for all s, problem (15) can be rewritten as

$$\begin{aligned} \max \ & \sum_{\forall s \in \mathcal{S}} w_{s,t} B (\alpha_s^{(k)} + \beta_s^{(k)} \tilde{\gamma}_s) \\ \text{s. t. } & \log\Big(\sum_{\forall s' \neq s, s' \in \mathcal{S}} \frac{g_{s'm_{s,t}^{*(k)},t} \beta_s^{(k)}}{g_{sm_{s,t}^{*(k)},t}} \exp(\tilde{P}_{s',t} + \tilde{\gamma}_s - \tilde{P}_{s,t}) \\ & \quad + \frac{\beta_s^{(k)} n_{m_{s,t}^{*(k)}}}{g_{sm_{s,t}^{*(k)},t}} \exp(\tilde{\gamma}_s - \tilde{P}_{s,t}) \Big) \leq 1, \quad \forall s \in \mathcal{S}, \\ & \tilde{P}_{s,t} \leq \log(P_{s,\max}), \quad \forall s \in \mathcal{S}, \\ \text{var. } & P_{s,t}, \quad \forall s \in \mathcal{S} \end{aligned} \tag{27}$$

Due to the linear objective function and the strictly convex constraint functions, problem (27) (and hence problem (15)) has a unique optimal solution. By [33, Proposition 3], this implies that Procedure 1 can globally converges to the optimal solution to problem (15). Therefore, Theorem 3 follows. ■

E. Proof of Theorem 4

For the natation brevity, we let $f_s(\boldsymbol{P}_t) = w_{s,t} B \log(1 + \max_{\forall m \in \mathcal{U}_{s,t}} \frac{P_{s,t} g_{sm,t}}{\sum_{\forall s' \neq s, s' \in \mathcal{S}} g_{s'm,t} P_{s',t} + n_m})$ and $\tilde{f}_s(\boldsymbol{P}_t) = w_{s,t} B (\alpha_s^{(l)} + \beta_s^{(l)} \log \frac{P_{s,t} g_{sm_{s,t}^{*(l)},t} / \beta_s^{(l)}}{\sum_{\forall s' \neq s, s' \in \mathcal{S}} g_{s'm_{s,t}^{*(l)},t} P_{s',t} + n_{m_{s,t}^{*(l)}}})$. Due to the maximum nature of SINR term in the function $f_s(\cdot)$, we have

$$f_i(\boldsymbol{P}_t) \geq \underbrace{w_{s,t} B \log(1 + \frac{P_{s,t} g_{sm_{s,t}^{*(l)},t}}{\sum_{\forall s' \neq s, s' \in \mathcal{S}} g_{s'm_{s,t}^{*(l)},t} P_{s',t} + n_{m_{s,t}^{*(l)}}})}_{\tilde{f}_s(\boldsymbol{P}_t)}. \tag{28}$$

By the inequality of arithmetic and geometric means, we further have $\bar{f}_s(\boldsymbol{P}_t) \geq \tilde{f}_s(\boldsymbol{P}_t)$ for all s. Together with (28), this implies that $f_s(\boldsymbol{P}_t) \geq \tilde{f}_s(\boldsymbol{P}_t)$ for all s. It follows that

$$\sum_{\forall s \in \mathcal{S}} f_s(\boldsymbol{P}_t) \geq \sum_{\forall s \in \mathcal{S}} \tilde{f}_s(\boldsymbol{P}_t) \tag{29}$$

for all feasible $\boldsymbol{P}_t$. By the values of $m_{s,t}^{*(l)}$'s, $\alpha_s^{(l)}$'s, and $\beta_s^{(l)}$'s, we can further get

$$\sum_{\forall s \in \mathcal{S}} f_s(\boldsymbol{P}_t^{(l)}) = \sum_{\forall s \in \mathcal{S}} \tilde{f}_s(\boldsymbol{P}_t^{(l)}) \tag{30}$$

and

$$\sum_{\forall s \in \mathcal{S}} \nabla f_s(\boldsymbol{P}_t^{(l)}) = \sum_{\forall s \in \mathcal{S}} \nabla \tilde{f}_s(\boldsymbol{P}_t^{(l)}) \tag{31}$$

where $\nabla f_s(\boldsymbol{P}_t^{(l)})$ and $\nabla \tilde{f}_s(\boldsymbol{P}_t^{(l)})$ mean the first-order derivative of functions $f_s(\boldsymbol{P}_t)$ and $\tilde{f}_s(\boldsymbol{P}_t)$ at the point $\boldsymbol{P}_t^{(l)}$, respectively. By Theorem 2, $\boldsymbol{P}_t^{(l)}$ is the globally optimal solution of maximizing $\tilde{f}_s(\boldsymbol{P}_t)$ in problem (15). By [34, Th. 1], three conditions (29)-(31) therefore implies that the solutions to a series of approximation problems (15) can converge to a point satisfying the necessary KKT optimality conditions of problem (14), and Theorem 4 follows. ■

REFERENCES

[1] N. Zhang, N. Cheng, A. T. Gamage, K. Zhang, J. W. Mark, and X. Shen, "Cloud assisted HetNets toward 5G wireless networks," *IEEE Commun. Mag.*, vol. 53, no. 6, pp. 59–65, Jun. 2015.

[2] Y. Mao, Y. Luo, J. Zhang, and K. B. Letaief, "Energy harvesting small cell networks: Feasibility, deployment, and operation," *IEEE Commun. Mag.*, vol. 53, no. 6, pp. 94–101, Jun. 2015.

[3] C. Wang, J. Li, and M. Guizani, "Cooperation for spectral and energy efficiency in ultra-dense small cell networks," *IEEE Wireless Commun.*, vol. 23, no. 1, pp. 64–71, Feb. 2016.

[4] S. Zhang, N. Zhang, S. Zhou, J. Gong, Z. Niu, and X. Shen, "Energy-aware traffic offloading for green heterogeneous networks," *IEEE J. Sel. Areas Commun.*, vol. 34, no. 5, pp. 1116–1129, May 2016.

[5] L. P. Qian, Y. J. A. Zhang, Y. Wu, and J. Chen, "Joint base station association and power control via Benders' decomposition," *IEEE Trans. Wireless Commun.*, vol. 12, no. 4, pp. 1651–1665, Apr. 2013.

[6] Y. Wu, K. Guo, J. Huang, and X. S. Shen, "Secrecy-based energy-efficient data offloading via dual connectivity over unlicensed spectrums," *IEEE J. Sel. Areas Commun.*, vol. 34, no. 12, pp. 3252–3270, Dec. 2016.

[7] T. H. Luan, R. Lu, X. Shen, and F. Bai, "Social on the road: Enabling secure and efficient social networking on highways," *IEEE Wireless Commun.*, vol. 22, no. 1, pp. 44–51, Feb. 2015.

[8] Q. Zheng, K. Zheng, H. Zhang, and V. C. M. Leung, "Delay-optimal virtualized radio resource scheduling in software-defined vehicular networks via stochastic learning," *IEEE Trans. Veh. Technol.*, vol. 65, no. 10, pp. 7857–7867, Oct. 2016.

[9] X. Ge, H. Chen, G. Mao, Y. Yang, and S. Tu, "Vehicular communications for 5G cooperative small-cell networks," *IEEE Trans. Veh. Technol.*, vol. 65, no. 10, pp. 7882–7894, Oct. 2016.

[10] Y. Saito, Y. Kishiyama, A. Benjebbour, T. Nakamura, A. Li, and K. Higuchi, "Non-orthogonal multiple access (NOMA) for cellular future radio access," in *Proc. IEEE VTC Spring*, Jun. 2013, pp. 1–5.

[11] L. Dai, B. Wang, Y. Yuan, S. Han, C.-L. I, and Z. Wang, "Non-orthogonal multiple access for 5G: Solutions, challenges, opportunities, and future research trends," *IEEE Commun. Mag.*, vol. 53, no. 9, pp. 74–81, Sep. 2015.
[12] D. Liu *et al.*, "User association in 5G networks: A survey and an outlook," *IEEE Trans. Commun. Surveys Tuts.*, vol. 18, no. 2, pp. 1018–1044, 2nd Quart., 2016.
[13] M. Tao, Y.-C. Liang, and F. Zhang, "Resource allocation for delay differentiated traffic in multiuser OFDM systems," *IEEE Trans. Wireless Commun.*, vol. 7, no. 6, pp. 2190–2201, Jun. 2008.
[14] S. Sadr and R. S. Adve, "Handoff rate and coverage analysis in multi-tier heterogeneous networks," *IEEE Trans. Wireless Commun.*, vol. 14, no. 5, pp. 2626–2638, May 2015.
[15] P. Xu, Z. Ding, X. Dai, and H. V. Poor. (2015). "NOMA: An information theoretic perspective." [Online]. Available: http://arxiv.org/abs/1504.07751
[16] J. Choi, "Non-orthogonal multiple access in downlink coordinated two-point systems," *IEEE Commun. Lett.*, vol. 18, no. 2, pp. 313–316, Feb. 2014.
[17] Z. Ding, Z. Yang, P. Fan, and H. V. Poor, "On the performance of non-orthogonal multiple access in 5G systems with randomly deployed users," *IEEE Signal Process. Lett.*, vol. 21, no. 12, pp. 1501–1505, Dec. 2014.
[18] Z. Ding, P. Fan, and H. V. Poor, "Impact of user pairing on 5G nonorthogonal multiple-access downlink transmissions," *IEEE Trans. Veh. Technol.*, vol. 65, no. 8, pp. 6010–6023, Aug. 2016.
[19] L. Lei, D. Yuan, C. K. Ho, and S. Sun, "Joint optimization of power and channel allocation with non-orthogonal multiple access for 5G cellular systems," in *Proc. GLOBECOM*, San Diego, CA, USA, Dec. 2015, pp. 1–6.
[20] S. Timotheou and I. Krikidis, "Fairness for non-orthogonal multiple access in 5G systems," *IEEE Signal Process. Lett.*, vol. 22, no. 10, pp. 1647–1651, Oct. 2015.
[21] M. Mollanoori and M. Ghaderi, "Uplink scheduling in wireless networks with successive interference cancellation," *IEEE Trans. Mobile Comput.*, vol. 13, no. 5, pp. 1132–1144, May 2014.
[22] W. Bao and B. Liang, "Stochastic geometric analysis of user mobility in heterogeneous wireless networks," *IEEE J. Sel. Areas Commun.*, vol. 33, no. 10, pp. 2212–2225, Oct. 2015.
[23] I.-W. Wu, W.-S. Chen, H.-E. Liao, and F. F. Young, "A seamless handoff approach of Mobile IP protocol for mobile wireless data networks," *IEEE Trans. Consum. Electron.*, vol. 48, no. 2, pp. 335–344, May 2002.
[24] W. Zhao and J. Xie, "A novel Xcast-based caching architecture for inter-gateway handoffs in infrastructure wireless mesh networks," in *Proc. IEEE INFOCOM*, Apr. 2009, pp. 1–9.
[25] R. Arshad, H. ElSawy, S. Sorour, T. Y. Al-Naffouri, and M.-S. Alouini. (Sep. 2016). "Velocity-aware handover management in two-tier cellular networks." [Online]. Available: http://arxiv.org/abs/1609.02411
[26] L. Qiang, J. Li, and C. Touati, "A user centered multi-objective handoff scheme for hybrid 5G environments," *IEEE Trans. Emerg. Topics Comput.*, vol. PP, no. 99, pp. 1–1, Apr. 2016.
[27] B. Fang and W. Zhou, "Handover reduction via joint bandwidth allocation and CAC in randomly distributed HCNs," *IEEE Commun. Lett.*, vol. 19, no. 7, pp. 1209–1212, Jul. 2015.
[28] L. Qin and D. Zhao, "Channel time allocations and handoff management for fair throughput in wireless mesh networks," *IEEE Trans. Veh. Technol.*, vol. 64, no. 1, pp. 315–326, Jan. 2015.
[29] A. L. Stolyar, "On the asymptotic optimality of the gradient scheduling algorithm for multiuser throughput allocation," *Oper. Res.*, vol. 53, no. 1, pp. 12–25, Jan. 2005.
[30] S. Boyd and L. Vandenberghe, *Convex Optimization*. Cambridge, U.K.: Cambridge Univ. Press, 2004.
[31] Y. J. Zhang, L. P. Qian, and J. Huang, "Monotonic optimization in communication and networking systems," *Found. Trends Netw.*, vol. 7, no. 1, pp. 1–75, Oct. 2013.
[32] M. Chiang, C. W. Tan, D. P. Palomar, D. O'Neill, and D. Julian, "Power control by geometric programming," *IEEE Trans. Wireless Commun.*, vol. 6, no. 7, pp. 2640–2651, Jul. 2007.
[33] J. Huang, R. A. Berry, and M. L. Honig, "Distributed interference compensation for wireless networks," *IEEE J. Sel. Areas Commun.*, vol. 24, no. 5, pp. 1074–1084, May 2006.
[34] B. R. Marks and G. P. Wright, "A general inner approximation algorithm for nonconvex mathematical programs," *Oper. Res.*, vol. 26, no. 4, pp. 681–683, 1978.
[35] *LTE; Evolved Universal Terrestrial Radio Access (E-UTRA); Radio Frequency (RF) requirements for LTE Pico Node B, Release 9*, document TR36.931, V9.0.0, 3GPP, May 2011.
[36] D. Tse and P. Viswanath, *Fundamentals of Wireless Communication*. Cambridge, U.K.: Cambridge Univ. Press, 2005.
[37] M. A. Taubenblatt, "Optical interconnects for high-performance computing," *J. Lightw. Technol.*, vol. 30, no. 4, pp. 448–458, Feb. 15, 2012.
[38] C. Develder *et al.*, "Optical networks for grid and cloud computing applications," *Proc. IEEE*, vol. 100, no. 5, pp. 1149–1167, May 2012.

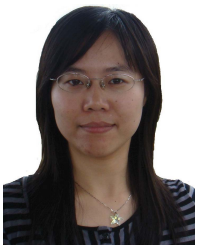

Li Ping Qian (S'08–M'10–SM'16) received the Ph.D. degree in information engineering from The Chinese University of Hong Kong, Hong Kong, in 2010. She was a Visiting Student with Princeton University in 2009. From 2010 to 2011, she was a Post-Doctoral Research Assistant with the Department of Information Engineering, The Chinese University of Hong Kong. She was with Broadband Communications Research Laboratory, University of Waterloo, from 2016 to 2017. She is currently an Associate Professor with the College of Information Engineering, Zhejiang University of Technology, China. Her research interests lie in the areas of wireless communication and networking, cognitive networks, and smart grids, including power control, adaptive resource allocation, cooperative communications, interference cancellation for wireless networks, and demand response management for smart grids.

Dr. Qian was a co-recipient of the IEEE Marconi Prize Paper Award in wireless communications (the Annual Best Paper Award of the IEEE TRANSACTIONS ON WIRELESS COMMUNICATIONS) in 2011, the Second-Class Outstanding Research Award for Zhejiang Provincial Universities, China, in 2012, the Second-class Award of Science and Technology given by Zhejiang Provincial Government in 2015, and the Best Paper Award from ICC 2016. She was also a Finalist of the Hong Kong Young Scientist Award in 2011, and a recipient of the scholarship under the State Scholarship Fund of China Scholarship Council for Visiting Scholars in 2015 and Zhejiang Provincial Natural Science Foundation for Distinguished Young Scholars in 2015. She serves as an Associate Editor of the *IET Communications*.

Yuan Wu (S'08–M'10–SM'16) received the Ph.D. degree in electronic and computer engineering from The Hong Kong University of Science and Technology, Hong Kong, in 2010. From 2010 to 2011, he was a Post-Doctoral Research Associate with The Hong Kong University of Science and Technology. From 2016 to 2017, he was a Visiting Scholar with the Broadband Communications Research Group, Department of Electrical and Computer Engineering, University of Waterloo, Canada. He is currently an Associate Professor with the College of Information Engineering, Zhejiang University of Technology, Hangzhou, China. His research interests focus on radio resource allocations for wireless communications and networks, and smart grid. He was a recipient of the Best Paper Award in IEEE International Conference on Communications in 2016.

Haibo Zhou (M'14) received the Ph.D. degree in information and communication engineering from Shanghai Jiao Tong University, Shanghai, China, in 2014. Since 2014, he has been a Post-Doctoral Fellow with the Broadband Communications Research Group, ECE Department, University of Waterloo. His research interests include resource management, and protocol design in cognitive radio networks and vehicular networks.

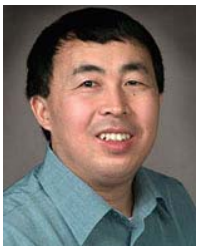

Xuemin (Sherman) Shen (M'97–SM'02–F'09) received the B.Sc. degree from Dalian Maritime University, China, in 1982, and the M.Sc. and Ph.D. degrees from Rutgers University, New Brunswick, NJ, USA, in 1987 and 1990, respectively, all in electrical engineering. He is currently a Professor and the University Research Chair with the Department of Electrical and Computer Engineering, University of Waterloo, Canada. He is also the Associate Chair for Graduate Studies. His research focuses on resource management in wireless networks, wireless network security, social networks, smart grid, and vehicular ad hoc and sensor networks. He is a registered Professional Engineer of Ontario, Canada, an Engineering Institute of Canada Fellow, a Canadian Academy of Engineering Fellow, a Royal Society of Canada Fellow, and a Distinguished Lecturer of the IEEE Vehicular Technology Society and Communications Society. He was an elected member of the IEEE ComSoc Board of Governor. He received the Excellent Graduate Supervision Award in 2006 from the University of Waterloo and the Premier's Research Excellence Award in 2003 from the Province of Ontario, Canada. He was the Chair of the Distinguished Lecturers Selection Committee. He served as the Technical Program Committee Chair/Co-Chair of the IEEE Globecom'16, the Infocom'14, the IEEE VTC'10 Fall, and the Globecom'07, the Symposia Chair of the IEEE ICC'10, the Tutorial Chair of the IEEE VTC'11 Spring and the IEEE ICC'08, the General Co-Chair of the ACM Mobihoc'15, and the Chair of the IEEE Communications Society Technical Committee on Wireless Communications, and P2P Communications and Networking. He also serves/served as the Editor-in- Chief of the IEEE NETWORK, the *Peer-to-Peer Networking and Application*, the *IET Communications*, and the IEEE INTERNET OF THINGS JOURNAL, a Founding Area Editor of the IEEE TRANSACTIONS ON WIRELESS COMMUNICATIONS, an Associate Editor of the IEEE TRANSACTIONS ON VEHICULAR TECHNOLOGY, *Computer Networks*, and the *ACM/Wireless Networks*, and the Guest Editor of the IEEE JSAC, the IEEE WIRELESS COMMUNICATIONS, the *IEEE Communications Magazine*, and the *ACM Mobile Networks and Applications*.